



Morphological comparison of distributed volcanic fields in the Main Ethiopian Rift using high-resolution digital elevation models

Jonathan A. Hunt ^{*}, Tamsin A. Mather, David M. Pyle

COMET, Department of Earth Sciences, University of Oxford, South Parks Road, Oxford OX1 3AN, UK

ARTICLE INFO

Article history:

Received 28 June 2019

Received in revised form 10 November 2019

Accepted 14 November 2019

Available online 4 December 2019

ABSTRACT

Distributed volcanic fields of scoria cones, maars, tuff cones and lava flows represent a crucial expression of the interplay between magmatism, tectonics and surface processes in continental rifts. We compare the cone morphology of two fields (Butajira and East Ziway) in the Main Ethiopian Rift (MER), using high-resolution digital elevation models (DEMs) to investigate volumes, surface environment and age of emplacement. Volumes of individual cones are similar in both fields (mean $\sim 4 \times 10^6 \text{ m}^3$) and lower than in other distributed volcanic fields located in extensional environments. Volcanism at Butajira has created linear clusters of superimposed cones, suggesting a small number of larger (10^7 – 10^8 m^3) fissure eruptions compared to the isolated events at East Ziway. The presence of maars and deep craters within cones at Butajira indicates phreatomagmatic activity, not seen at East Ziway where cones may have been emplaced during a dry climate phase. Shape parameters, including curvature of cone rims and ratios of cone height, width and crater depth, suggest younger eruption ages at Butajira compared to East Ziway and the possibility of ongoing activity in this area. A broader survey of cone fields across the MER using the ASTER global digital elevation model fails to identify systematic variation in height, width and volume from cone morphology, limited by low-resolution. High-resolution topography provides a useful insight into rift environments at the time of emplacement, and further surveys across the Main Ethiopian Rift may advance our understanding of distributed volcanism in extensional settings and the hazards they present.

© 2019 The Authors. Published by Elsevier B.V. This is an open access article under the CC BY license (<http://creativecommons.org/licenses/by/4.0/>).

1. Introduction

The interplay between magmatism and tectonics in continental rifts is a key relationship that governs rift architecture (e.g., Ebinger and Casey, 2001; Corti et al., 2003), extensional dynamics (e.g., Wright et al., 2006; Keir et al., 2006; Daniels et al., 2014), and the location and style of volcanism (e.g., Acocella et al., 2002; Abebe et al., 2007). In continental rifts, extension is driven by a large-scale stress regime interacting with multiple generations of new or inherited crustal structures (e.g., Corti et al., 2018a). Melt generation (e.g., Armitage et al., 2010; Ferguson et al., 2013) and dike intrusion (e.g., Keir et al., 2009) provide frequent opportunities for small-volume basaltic volcanism. Distributed volcanic fields are a common expression of this relationship in extensional environments (e.g., Connor and Conway, 2000; Michon and Merle, 2001; Hughes et al., 2002; Le Corvec et al., 2013a), comprising spatially dispersed, small-volume and usually mafic scoria deposits with individual vents (e.g., Smith and Németh, 2017). Such fields are

commonly referred to as “monogenetic” volcanic fields, though formation from single eruptions is often difficult to verify.

The deposits create a range of land forms (scoria cones, maars, tuff cones, and lava domes) with variable sizes, shapes and alignments depending on a number of internal and external factors. Internal factors include the physical and chemical properties of the magma, whilst external factors include the local stress regime, crustal structure, host rock and surface environment (e.g., Kereszturi et al., 2011; Smith and Németh, 2017). The surface environment of continental rifts is varied, with resurfacing by fresh volcanism and a changing hydrological cycle over time. Lakes, high surface run-off and high groundwater levels are common in rifts due to topography. All of these processes depend on the stage of rifting, as the continental rift progresses from inception to late stage extension (e.g., Hayward and Ebinger, 1996). The contexts in which monogenetic volcanic fields are formed in rifts are therefore rich and varied, leading to a wide variety in their geography and morphology.

The shape of distributed or monogenetic volcanic fields and the alignment of vents have been used to investigate magma transport (e.g., Connor et al., 1992; Condit and Connor, 1996; Paulsen and Wilson, 2010). Analysis of 37 monogenetic volcanic fields showed that magma transport depends on both deep level influences (e.g., magma

^{*} Corresponding author at: Department of Earth Sciences, University of Oxford, Oxford OX1 3AN, UK

E-mail addresses: jonathan.hunt@earth.ox.ac.uk (J.A. Hunt), tamsin.mather@earth.ox.ac.uk (T.A. Mather), david.pyle@earth.ox.ac.uk (D.M. Pyle).

source) and the shallow stress field and structures (Le Corvec et al., 2013a). Fields in extensional environments showed multiple orientations of volcanic alignments (Le Corvec et al., 2013a; Mazzarini et al., 2016), probably owing to the multiplicity in rift environments of crustal structures (Le Corvec et al., 2013b) and small-scale stress fields (e.g., due to segmentation, obliquity, and/or transfer zones; Corti, 2008; Muirhead et al., 2015).

Simple vent alignments may imply simple plumbing systems whereby single dikes propagate from depth for each eruptive episode in the field; however, observations of exposed networks of sills and dikes beneath monogenetic volcanic fields suggest complex plumbing systems (Muirhead et al., 2016). Petrology and pre-eruptive seismicity also suggest magma mixing and the possibility of multiple intrusions of melt before eruption (Albert et al., 2016).

Cone morphology has been used to investigate both internal and external conditions at time of emplacement, including changes in surface water (Risso et al., 2008; Kereszturi et al., 2011), tectonic activity (e.g., Tibaldi, 1995; Corazzato and Tibaldi, 2006), and physical and chemical properties of erupted material (e.g., Settle, 1979; Riedel et al., 2003; Bemis and Ferencz, 2017). Morphometry can also provide an indication of age due to degradation of the cones. A common approach is to use the ratio of height to width (H/W), which has been proposed to be approximately constant for fresh scoria cones (0.18; Porter, 1972; Wood, 1980a). Erosion of the scoria cone leads to a reduction in height and enlargement of the base, resulting in smaller H/W ratios for older ages (Settle, 1979; Wood, 1980b; Inbar et al., 2011).

However, H/W ratios depend on a large number of primary processes in addition to age (Favalli et al., 2009; Bemis and Ferencz, 2017). The exact method of calculating H/W may also influence the results, particularly if the cones have been emplaced on an inclined substrate and/or have been subsequently buried (Favalli et al., 2009). Further, the resolution of the elevation data used to calculate the H/W may result in bias (Fornaciai et al., 2012). Analysis of a large number of scoria cones from a range of geodynamic settings suggests that cones in extensional settings exhibit lower H/W and higher ratios of crater width to cone width (W_{cr}/W_{co}) compared to those in subduction settings (Fornaciai et al., 2012).

The morphology of small-volume, distributed volcanism in a rift environment therefore includes information on their age as well as extensional dynamics, eruption style and surface environment at time of emplacement. This study aims to compare the morphology of cones from two distributed volcanic fields in the Main Ethiopian Rift (MER) using high-resolution digital elevation models. We focus on three major influences on morphology: (1) eruption volume and mode of emplacement, (2) surface environment including local hydrology, and (3) relative age of cones. We also explore the capability of freely available low-resolution DEMs to compare the morphology of other volcanic fields across the rift.

1.1. Volcanic fields in the Main Ethiopian Rift

The extension which formed the Main Ethiopian Rift (MER) began in the Late Miocene, first creating large NE-SW faults, a series of asymmetric basins and widespread volcanic activity (WoldeGabriel et al., 1990; Corti, 2009). In the Late Pliocene, extension migrated from the rift border faults to an echelon, axial magmatic segments (Ebinger and Casey, 2001) due to progressive thinning of the lithosphere, weakening associated with magmatism and/or a change in rift kinematics (Wolfenden et al., 2004; Kendall et al., 2005; Corti, 2008, 2009). These two phases of rift development created the two systems of faults in the present-day MER: older NE-SW border faults and currently active NNE-SSW rift-floor faults (Keir et al., 2006).

Distributed volcanic fields are found within two fault belts in the central MER (Fig. 1; Mazzarini and Isola, 2010): on the west, the Silti-Debre Zeyit Fault Zone (SDFZ); on the east, the Wonji Fault Belt (WFB). The WFB runs along the eastern side of the central MER

(~7.5–8.5°N) and becomes the rift axis in the northern MER (~8.5–9.5°N). The major silicic centres within the MER are found within or closely associated with the WFB, with cone fields interspersed. The SDFZ is less seismically active (Keir et al., 2006) and hosts fewer faults than the WFB (Abebe et al., 2005), and is suggested to be a failed rift segment or an incipient zone of strain (Keir et al., 2006; Corti, 2009). The SDFZ includes volcanic fields near the major town of Bishoftu, and smaller towns of Butajira, Silti and Soddo (e.g., Rooney et al., 2011). Whilst the deposits (mostly scoria cones) are Quaternary to recent in age (<2 Ma; Chernet et al., 1998; Abebe et al., 2005), a cluster of cones further offset from the rift axis at Akaki are Pliocene-Quaternary (3–2 Ma; Mazzarini et al., 1999; Abebe et al., 2005) but are geochemically similar to the rest of the SDFZ (Rooney et al., 2014).

Cones in both the SDFZ and WFB are commonly located near or on top of extensional faults (Korme et al., 1997, 2004; Casey et al., 2006; Corti et al., 2013). The spatial distribution of both vents and faults in the MER displays self-similar (fractal) clustering, and the length-scales at which this clustering occurs is hypothesised to correlate with the depth from which dikes are fed (e.g., Mazzarini and Isola, 2010). Accordingly, the SDFZ is hypothesised to be fed by dikes from deeper in the crust than the WFB (Mazzarini and Isola, 2010; Mazzarini et al., 2013a). Similarities between the fractal behavior of earthquakes and that of vents throughout the MER suggest a genetic link between faults and vents (Mazzarini et al., 2013b).

Statistical analysis of the locations of vents within the Bishoftu (syn. Debre Zeyit), Wonji, Kone and Akaki fields suggests that the shape of each field is determined by large crustal structures (Mazzarini et al., 2016). Within fields closer to the rift axis, vent location is principally controlled by the state of stress and vents are therefore aligned with contemporaneous faults; further from the rift axis (i.e., SDFZ fields, particularly Akaki), vent location is controlled by pre-existing structures and border faults (Mazzarini et al., 2016; Corti et al., 2018b).

Geochemical analysis of lavas from the distributed volcanic fields suggests that SDFZ magmas are the result of lower degrees of melting and greater depths of differentiation than WFB lavas, with a fractionation system that is spread widely through the mid-lower crust (Rooney et al., 2005, 2007, 2011).

In this study we compare the morphology of distributed volcanism in two fields of the MER (Fig. 1): the Butajira field (within the SDFZ) and the East Ziway field (within the WFB). Both fields are at the same latitude in the central MER. The Butajira field is on the western flank of the rift, adjacent to the Guraghe border fault, within the Butajira marginal graben (WoldeGabriel et al., 1990; Corti et al., 2018a), and is situated close to a conductor imaged at depth by magnetotellurics (Hübert et al., 2018). The East Ziway field lies to the east of Lake Ziway and Aluto volcano, one of the most active silicic centers in the MER (Hutchison et al., 2016; McNamara et al., 2018; Fontijn et al., 2018). The WFB in this area is located on a west-dipping monocline, with rotation possibly due to magma intrusion (Corti et al., 2018a).

2. Methodology

2.1. High-resolution Pleiades digital elevation models (DEMs)

Very-high-resolution panchromatic (50-cm) and multispectral (2-m) orthoimages from the Pleiades-HR 1A satellite were obtained in stereo for the areas of Butajira and East Ziway (Fig. 1). The satellite data were processed using the Leica Photogrammetry Suite; the full methodology is detailed by Zhou et al. (2015). The use of stereo images to create a DEM works on the principle of parallax. Two images from different perspectives can be joined together with tie-points – the same feature identifiable in both orthoimages. Initial creation of a DEM using tie-points results in a point cloud with a variable spatial density.

Pleiades-derived DEMs have an average horizontal resolution of 1–2 m and vertical accuracy of ~0.3 m (according to comparison with LIDAR DEMs; Zhou et al., 2015), varying with point cloud density due

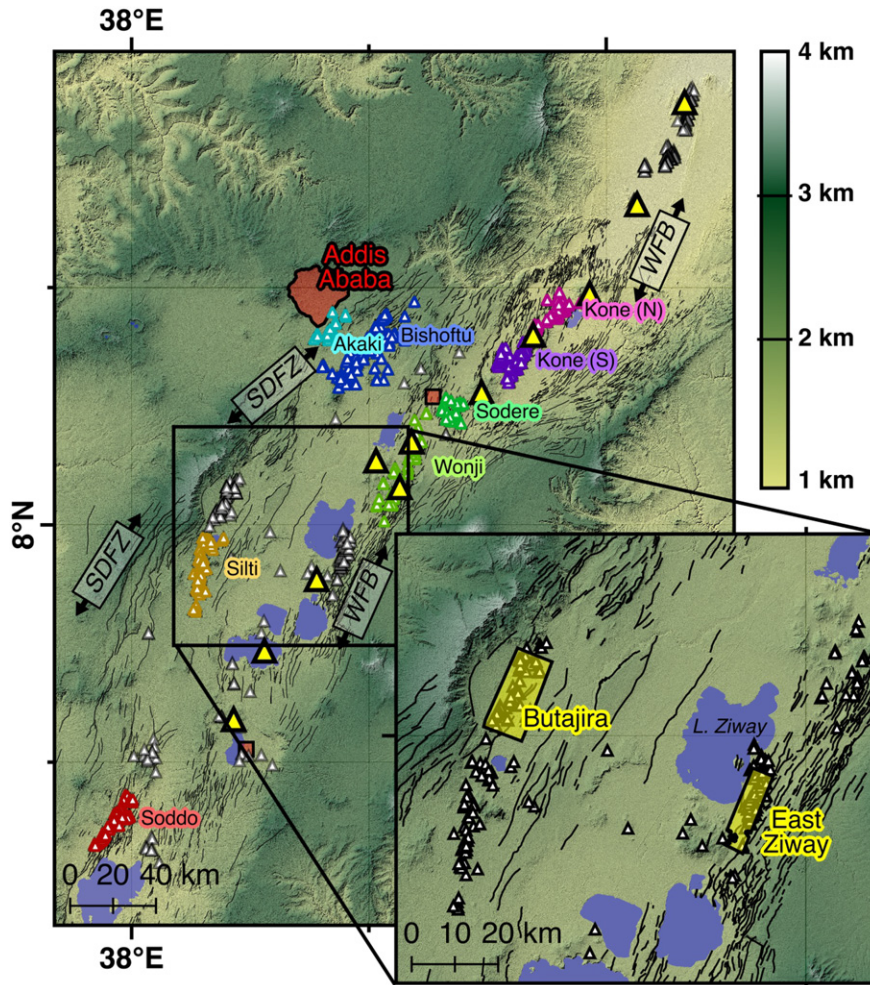


Fig. 1. Location map for the cone fields in this study. Elevation and hillshade provided by Aster GDEM (product of METI and NASA). Yellow triangles, major silicic centers; small triangles, volcanic cones (colored by field); red-filled squares/settlement outlines, cities of population >100,000; black lines, faults located in two major fault belts (SDFZ: Silti-Debre Zeyit Fault Zone; WFB: Wonji Fault Belt).

to lack/abundance of features and cloud cover. For analysis, it is convenient to regrid points using a block mean filter and an interpolation algorithm using continuous curvature splines, creating a regular grid of elevation values at 0.5-m spacing. Dense cloud cover must be removed from the point cloud. Cloud cover affects 2.1% of the stereo images for Butajira and 7.1% at East Ziway.

From these models and using QGIS (<http://www.qgis.org>), we manually mapped cones and maars in each volcanic field at a scale of 1:4000. We classified cones according to their regularity, extent of burial/erosion, and local geological context (e.g., nearby faults, associated lava flows, offset craters) in the following categories: partial/buried, dissected/eroded, breached/irregular and regular (see Figs. S1–S2). Cones are considered dissected/eroded if they are irregular on a small scale relative to the general cone shape and/or are influenced by linear channels/structures. Conversely, cones are considered breached/irregular if they are irregular on a large scale relative to the general cone shape and such irregularities are not linear.

To calculate volumes of deposits, the areal extent of each cone/maar was mapped on the basis of slope (below $\sim 3^\circ$). We generated an estimated basal topography by removing the data within the cone bounds and interpolating across the data gap, using the same surface gridding algorithm (continuous curvature splines) used in original DEM construction (Fig. 2a). By subtracting the basal topography from the unedited DEM, we created a new DEM of cone elevations (Fig. 2b). The new

DEM was used to calculate volumes from each separable deposit (i.e., whether clusters or isolated cones). We generated best fitting probability distributions to the volume data using MATLAB's fitdist function, with a non-parametric kernel-smoothing distribution and a normal kernel smoother.

For regular cones, morphometric parameters were calculated (see Table 1). A sub-circular base was drawn for each regular cone, excluding irregularities around the base of the cones (e.g., adjacent cones) that were captured in the original areal extent (green vs red polygons, Figs. S1–S2). Craters on regular cones were also mapped as enclosed polygons, in some cases extended across a crevasse breaching a part of the cone. From the sub-circular base and crater polygons, areas and average diameters were calculated (A_{co} , A_{cr} , W_{co} , W_{cr} ; Table 1). Maximum cone height (H_{max}), average height of cone rim (H_{co}) and depth of crater (D_{cr}) were calculated using the isolated DEMs of each cone after basal topography was removed.

In the case of overlapping cones, the DEM-differencing technique is unable to capture individual cone volumes. To overcome this, idealized volumes were calculated for regular cones using a simple geometry of an ideal cone on the basis of cone height and width, and crater width and depth (Fig. 2b, dashed line).

The curvature of the cone rims was calculated using a MATLAB script in which a 4th-degree polynomial was fit to 150-m sections of each profile (Fig. S3). The second derivatives of the polynomials then provided

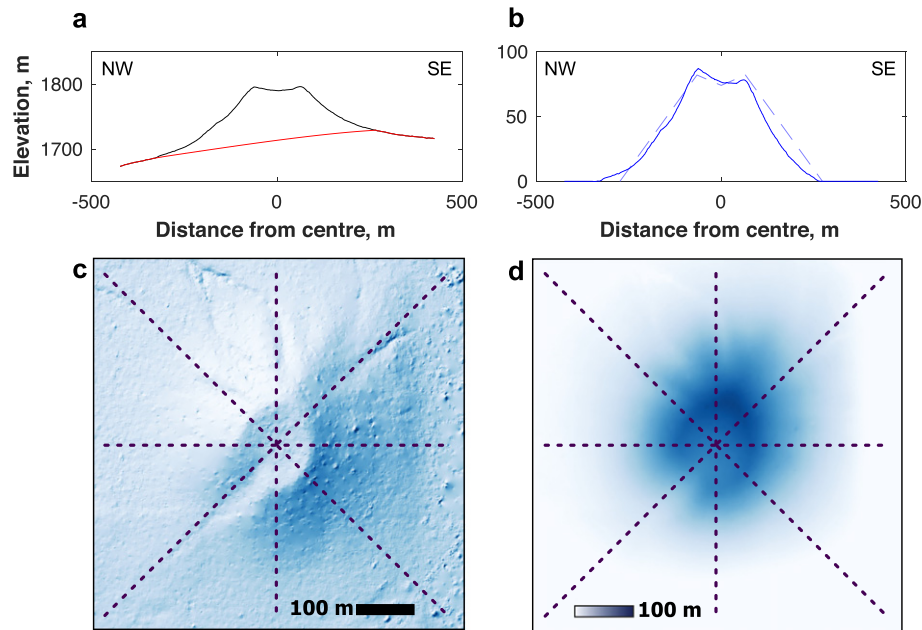


Fig. 2. Example of cone profiles and removal of interpolated base topography (from EZ28: East Ziway field, 7.8535°N 38.8785°E). (a) Profile from NW-SE of the cone: black = unedited DEM; red = interpolated basal topography. (b) Profile from NW-SE of the cone after removal of the basal topography: solid blue = edited DEM; dashed light blue = constructed visualization of ideal cone for V_{ideal} (using W_{co} , W_{cr} , H_{co} and D_{cr} ; see text, Table 1, and Supplementary Information S1). (c) Hillshade map of the cone from unedited DEM (solar azimuth 315°). (d) Elevation map of the cone after removal of the basal topography.

an estimate of the curvature of the cone rims (Fig. S4). Some cone rims were not accurately captured by the profile sections, and/or did not represent a point of greatest negative curvature – these were discarded.

2.2. Low-resolution ASTER GDEM

To extend our survey across the Main Ethiopian Rift, we used the freely downloadable ASTER Global DEM (GDEM; <http://www.gdem.aster.ersdac.or.jp>), a product of METI (Ministry of Economy, Trade, and Industry of Japan) and NASA (United States National Aeronautics and Space Administration). The ASTER GDEM has a resolution of 1 arc sec (~30 m) and typical accuracy of ± 1 pixel. Using the cone locations published in Mazzarini and Isola (2010) as a starting point, we mapped approximate bounds from the change in slope for cones in ten fields (Fig. 1): Soddo, Silti, Butajira, Bishoftu, Akaki, East Ziway, Wonji, Sodere, Kone (South) and Kone (North). Cones were selected on the basis of simple morphology and subcircular bases.

The resolution of the ASTER GDEM is insufficient to resolve crater width and depth. Cone width was calculated from the sub-circular polygons using the same method as the Pleiades analysis, and maximum heights and volumes were calculated using the same interpolation method to estimate basal topography (Table 1).

3. Results

3.1. Overview of morphology from Pleiades DEMs

Fig. 3 shows Pleiades-derived slope maps for the two study areas, Butajira and East Ziway, with cone bounds shown in red. Both fields contain ca. 50 cones (Table 2), that share a number of similar features. Cloud cover may obscure one or two cones, particularly in the south of the Butajira field.

The Butajira cones are found in clusters. Two linear clusters lie in the center and south of the field, with the northern cones forming a further two or three smaller clusters. In contrast, most cones in East Ziway are isolated from each other, with the exception of a ridge (Fig. 3d). Within this ridge, individual cones are indistinguishable, unlike the overlapping but distinct cones which form clusters in the Butajira field.

In central and southern Butajira, cone clusters lie parallel to a series of east-dipping rift-related normal faults at a distance of 2–3 km to the west (on the upthrown side). Similarly in the East Ziway field, many cones lie immediately to the west (upthrown side) of east-dipping fault scarps, particularly in the north of the field. The distance between faults and cones in the East Ziway field is far shorter than in Butajira, with many cones within 1 km of faults and a number lying along the

Table 1
Morphometric parameters calculated from the Pleiades DEMs and ASTER GDEM.

Parameter	Unit	Description
V	m^3	Cone volume calculated by the DEM differencing method between the original DEM and an interpolated pre-eruptive surface.
H_{max}	m	Maximum cone height above interpolated pre-eruptive surface.
H_{co}	m	Average height of cone rim above interpolated pre-eruptive surface, calculated from four profiles across the cone.
A_{co}	m^2	Planimetric area of the cone base (green polygons in Figs. S1–S2).
A_{cr}	m^2	Planimetric area of the cone crater, where applicable (blue polygons in Figs. S1–S2).
W_{co}	m	Average diameter of the cone base, calculated as $2\sqrt{A_{co}/\pi}$.
W_{cr}	m	Average diameter of the cone crater, calculated as $2\sqrt{A_{cr}/\pi}$.
D_{cr}	m	Elevation difference between cone rim and lowest point of crater, averaged for four profiles across the cone.
V_{ideal}	m^3	Idealized cone volume calculated from H_{co} , W_{co} , W_{cr} and D_{cr} .
H_{max}^{AS}	m	Maximum height of cones within bounds in analysis of the Aster GDEM.
W_{co}^{AS}	m	Average diameter of the cone base in analysis of the Aster GDEM, calculated in the same way as W_{co} .

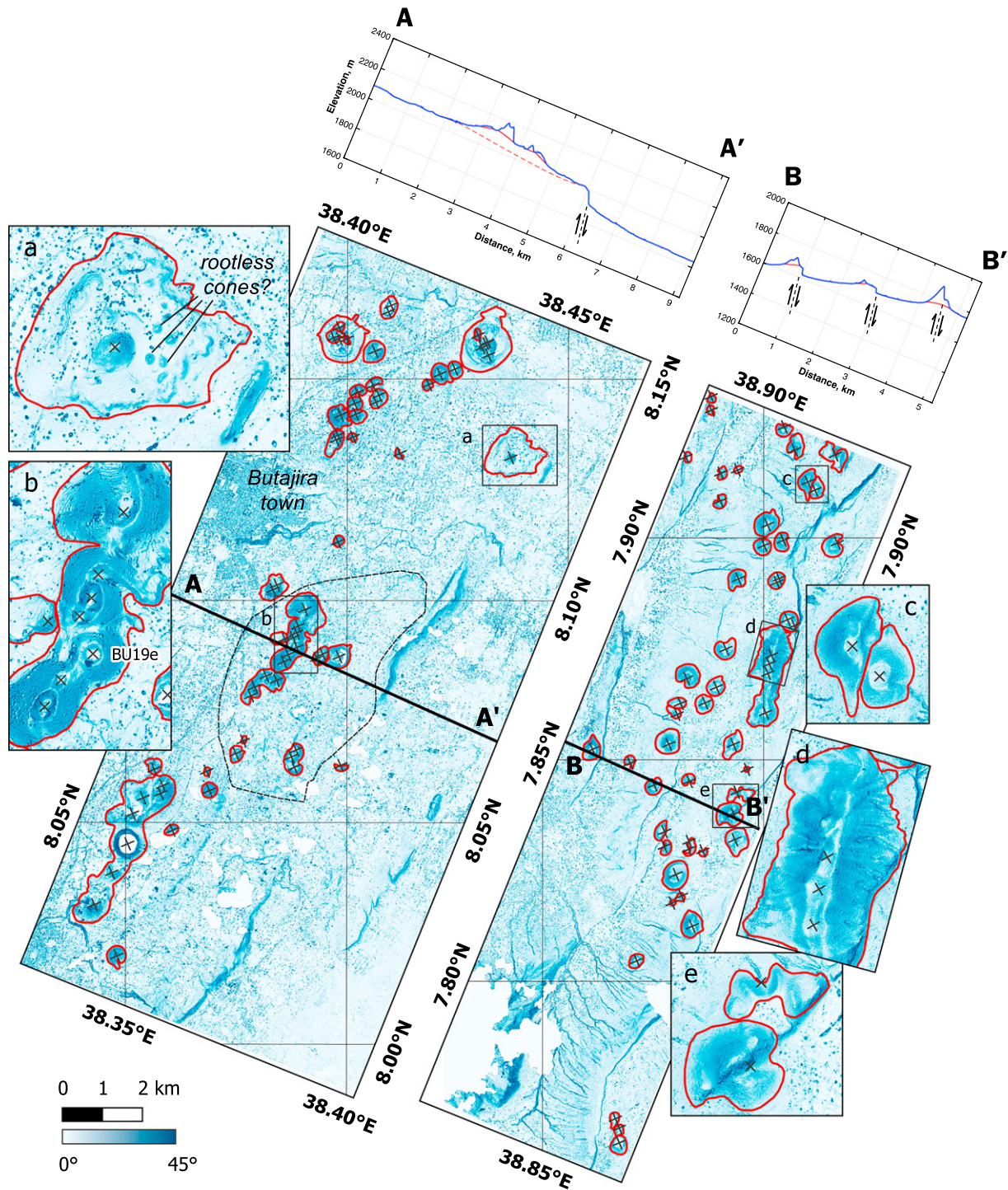


Fig. 3. Slope maps of the Butajira (left) and East Ziway (right) cone fields derived from Pleiades digital elevation models (DEMs). Cone centers are denoted by black crosses, and red lines mark the outer areas used to generate the basal topography and associated volumes for each mapped cone/cluster. Black dashed line demarks broad high associated with the central cluster. Elevation profiles across the cone fields are shown above (blue = unedited DEM, red = basal topography, dashed red = basal topography including broad high). (a)–(e) Zoom-in panels of particular features: (a) BU34 with associated lava flow and possible rootless cones; (b) Butajira cluster showing regular cone BU19e; (c) and (e) East Ziway examples of dissected cones; (d) East Ziway ridge (multiple rifted cone).

Table 2
Number of cones/maars in each category by field.

Cone field	Total cones/maars	Maars	Regular cones	Breached/irregular	Dissected/eroded	Partial/buried
Butajira	50	6	7	18	7	12
East Ziway	51	0	8	15	14	14

fault trace. In these cases, faults have cut through the cones, indicating fault activity post-emplacement.

Profiles across the cone fields (Fig. 3, upper panels) show the broader topographical context of the cones. In the Butajira field, cones are emplaced on a broad high formed by successive lava deposits, possibly related to the same fissure eruptions that formed the cones. A number of lava flow deposits related to cone emplacement can be identified on the basis of structural relationships and uneven topography at Butajira, particularly at the clusters in the center (Fig. 3b) and south of the field, and associated with two large maars in the north (Fig. S1). Lava flow deposits are less clear in the East Ziway field, where the topography is dominated by lake sediments, normal faults and river-cut channels. There are no clear examples of lava flows emanating from cones in the East Ziway field.

Table 2 lists the numbers of features recognized in the two cone fields by category, defined in Section 2.1. Cone types are broadly similar across the two fields, but maars have only been identified in Butajira. Several of the Butajira maars host cones emplaced after maar formation, along with associated lava flows. In the case of BU34, small cones are distributed across the area. The small size and high concentration, along with a broad high possibly indicating a lava flow, suggest that they may be rootless in origin (Fig. 3a; Fig. S1). Alternatively, they may be remnants of breached cones. More “breached/irregular” cones have been identified at Butajira, whereas more “dissected/eroded” cones have been mapped at East Ziway (Fig. S1–S2; Fig. 3c, Fig. 3e; Table 2, noting the similar total cones/maars in each field), although there could be some overlap between these definitions. “Dissected/eroded” cones in East Ziway may partly be a function of the more numerous faults at a closer proximity to cones.

Profiles drawn in four compass directions across regular cones are shown in Fig. 4. Regular cones in Butajira are more symmetrical than in East Ziway, where profiles commonly vary dependent on orientation. Craters are shallow or absent in East Ziway and are deeper in Butajira, with crater depth as much as 40–70% of cone height in three cases.

Cone rims are sharper on regular cones in Butajira than they are in East Ziway, as shown by with a greater negative curvature (Fig. 4b).

3.2. Volumes and morphometric parameters from Pleiades DEMs

The volumes calculated using the DEM differencing technique on the Pleiades-derived DEMs are plotted in Fig. 5. The clustered cones in the Butajira field are inseparable – the volumes of the clusters are plotted instead of individual cones. Most cone volumes, excluding the “partial/buried” category, are from 10^6 to 10^7 m³.

The probability distributions show positive skew. Average cone volumes in Butajira (median = 4.1×10^6 m³; mean = 4.2×10^6 m³) are higher than those in East Ziway (median = 3.2×10^6 m³; mean = 3.8×10^6 m³). When “regular”, “breached/irregular” and “dissected/eroded” cones are considered (dot/dashed lines), volumes of cones in East Ziway are bimodal. Butajira cone volumes are unimodal, except when including “partial/buried” cones. In both cases, inclusion of the “partial/buried” category shifts the distribution significantly to lower values. Analysis of the combined volume data provides a combined probability distribution with a median cone/maar volume of 3.4×10^6 m³ and a mean of 4.0×10^6 m³. In Butajira, the volume of the broad topographic high associated with the central cluster and associated lava flows is estimated as $\sim 4.6 \times 10^8$ m³ (see Fig. 3 and Fig. S5 for a map and bounds).

Idealized volumes calculated for “regular” cones using cone heights/widths (H_{co} , W_{co}) and crater widths/depths (W_{cr} , D_{cr}) allow the comparison of volumes of isolated cones with those that form part of a cluster (which would otherwise be inseparable; e.g., BU19e, Fig. 3b). The idealized volumes reproduce DEM-calculated volumes within 10% and relative volume differences between isolated cones (Supplementary information S2, Fig. S6).

In Fig. 6, the morphometric ratio H_{max}/W_{co} is plotted against V_{ideal} , W_{cr}/W_{co} and D_{cr}/H_{co} (see Table 1 for definitions) for the Butajira and East Ziway fields. The fields are largely separable on the basis of the

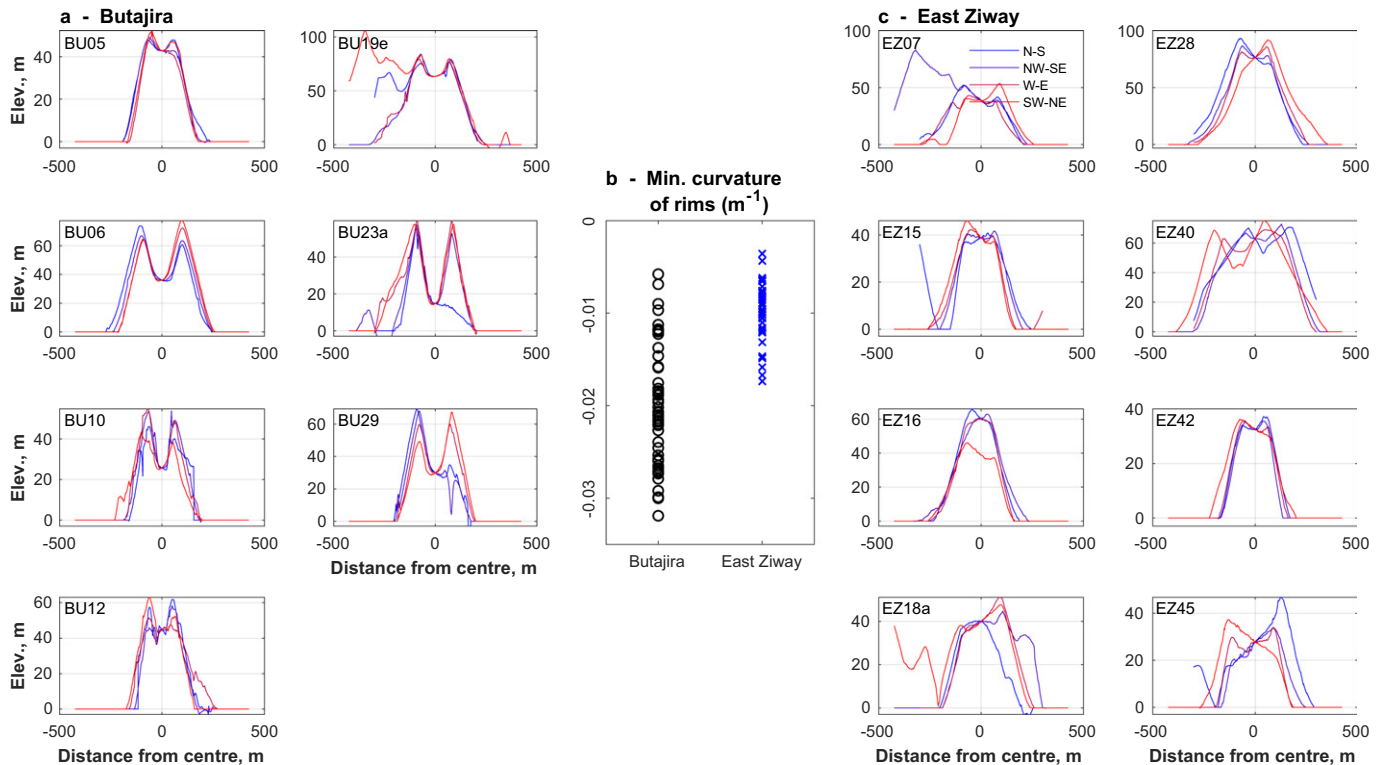


Fig. 4. (a) and (c) Profiles of regular cones from Butajira and East Ziway. Cone IDs correspond to those in Fig. S1 and Fig. S2. (b) Minimum curvature of cone rims at Butajira and East Ziway, see Fig. S4 for best-fitting polynomials and Fig. S5 for second derivatives.

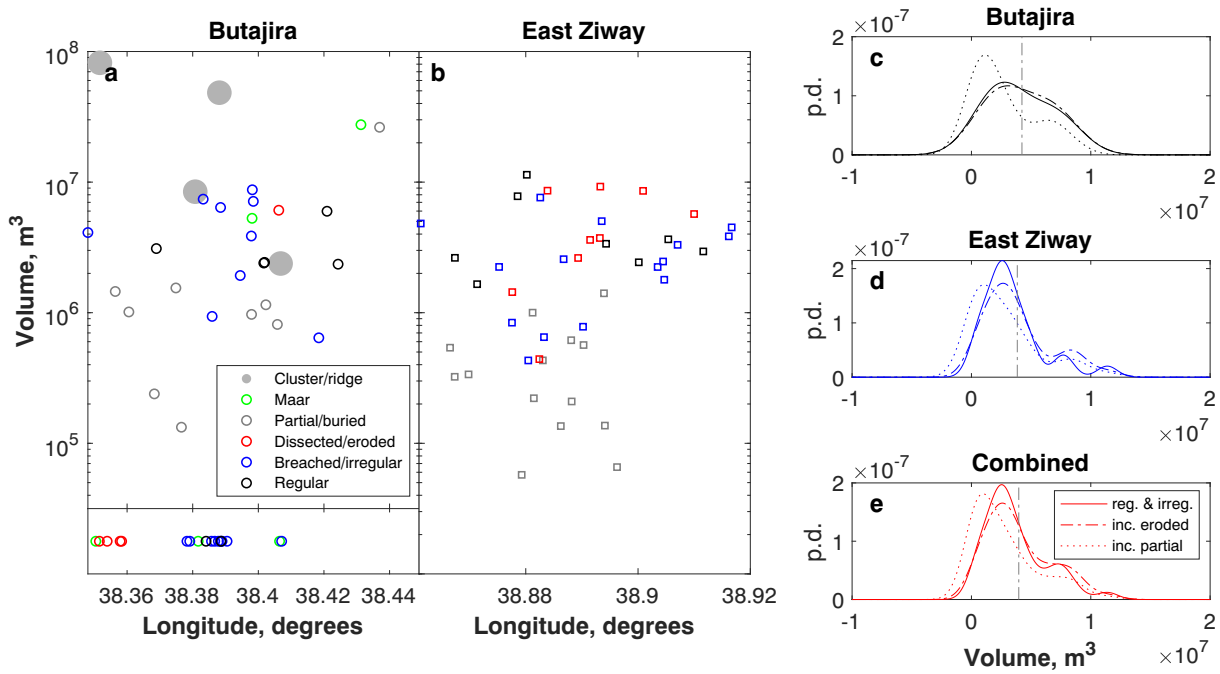


Fig. 5. (a)–(b) Volumes of maars, cones and associated deposits from Butajira (a, circles) and East Ziway (b, squares). At Butajira, numerous cones and maars form inseparable clusters/ridges – the locations of these are plotted in the box below (a) and combined volumes are plotted as solid grey circles. (c)–(e) Probability distributions of cone/maar volumes for Butajira, East Ziway and the combined dataset (p.d. = probability density) for three sets of data each: (1 – solid line) “regular” and “breached/irregular”; (2 – dot/dashed line) additionally including the “dissected/eroded” category; and (3 – dotted line) additionally including the “partial/buried” category. Vertical grey line shows the mean for set (2).

H_{max}/W_{co} ratio: Butajira cones have larger ratios than East Ziway cones, except for EZ28. There is a large scatter in these ratios which range between 0.1 and 0.21, either side of the average for fresh cones of 0.18 (Porter, 1972; Wood, 1980a). Three Butajira cones have greater ratios than this global average.

There is a large overlap in V_{ideal} except for two outliers in the East Ziway field, EZ28 and EZ40. The values of W_{cr}/W_{co} are also indistinguishable between the two fields, except for EZ28, and are broadly consistent with the average for fresh cones of 0.4 (Porter, 1972; Wood, 1980a). The fields are mostly separable on the basis of D_{cr}/H_{co} , with high ratios typifying the deep craters of Butajira cones compared to those of East Ziway. However, a number of Butajira cones overlap with the range of D_{cr}/H_{co} values from East Ziway.

3.3. Morphometric parameters from ASTER global digital elevation model (GDEM)

Morphometric parameters H_{max}^{AS} and W_{co}^{AS} (defined in Table 1) are plotted in Fig. S7, as well as volumes calculated from DEM-differencing using the ASTER GDEM. The average H_{max}^{AS}/W_{co}^{AS} is 0.148 with most cones below the average for fresh cones of 0.18 (Porter, 1972; Wood, 1980a). There is a positive correlation between the ratio H_{max}^{AS}/W_{co}^{AS} and volume.

The results from selected fields are presented in Fig. 7. The Wonji cone field exhibits a larger range of H_{max}^{AS} and W_{co}^{AS} and is responsible for many of the extreme values in the population. The cone fields at Bishoftu and north and south of Kone Caldera Complex are distinguishable by lower volumes and a more

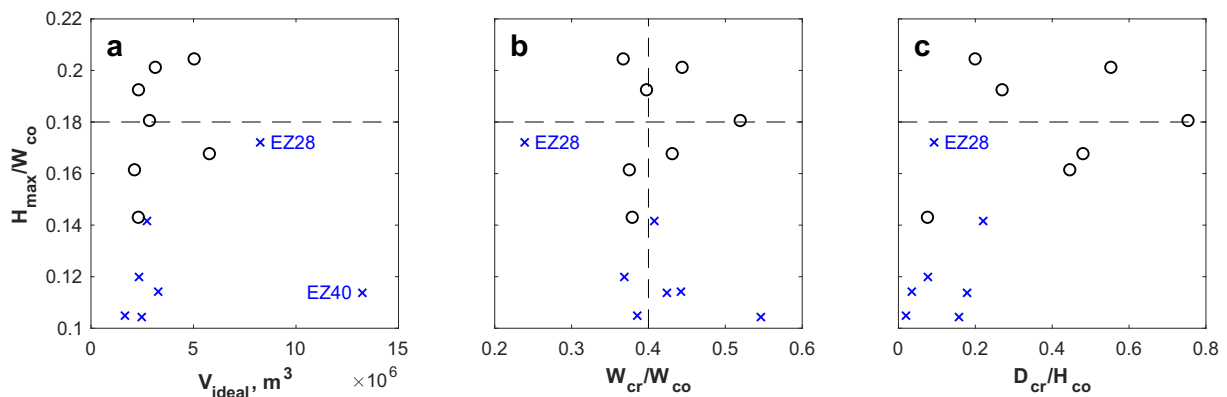


Fig. 6. H_{max}/W_{co} of “regular” cones against (a) idealized volume, (b) W_{cr}/W_{co} , and (c) D_{cr}/H_{co} (see Table 1 for definitions). Cone EZ16 does not have a crater and is therefore not included in the plots. Black circles = Butajira; blue crosses = East Ziway. Dashed lines are shown for average values for fresh scoria cones: $H_{max}/W_{co} = 0.18$ and $W_{cr}/W_{co} = 0.4$ (Porter, 1972; Wood, 1980a).

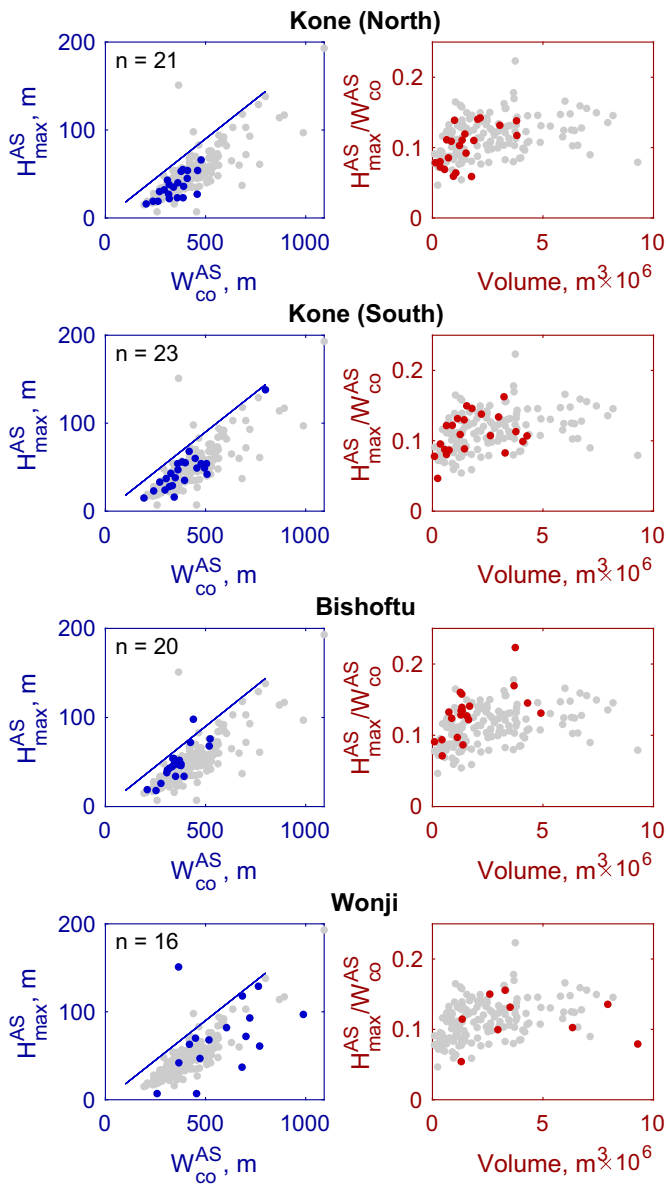


Fig. 7. Results from the analysis of ten cone fields (Fig. 1) across the Main Ethiopian Rift using the ASTER GDEM. The total set of results from the analysis are shown in grey (see Fig. S8).

restricted range of H_{max}^{AS} and W_{co}^{AS} , together responsible for the low volume–high H_{max}^{AS}/W_{co}^{AS} values in the population.

4. Discussion

4.1. Comparison of the Butajira and East Ziway fields

Our digital elevation models highlight several key differences between the Butajira and East Ziway cone fields. At Butajira, cones are found in linear clusters with associated lava flows, approximately 2 km west of nearby east-dipping faults. At East Ziway, isolated cones are found on or immediately adjacent to pervasive faulting. As a consequence, there are more dissected cones in East Ziway than in Butajira, where maars and breached/irregularly-formed cones are common. Cones in Butajira have sharper rims and larger H_{max}/W_{co} and D_{cr}/H_{co} ratios than those in East Ziway (Fig. 4, Fig. 6, Table 1 for definitions).

Multiple factors influence these morphometric and geospatial differences between cone fields (see Section 1). In this section we discuss (1) eruption volumes and modes of emplacement, including the role

of dikes, faults and plumbing systems; (2) surface environment, namely local hydrology; and (3) relative age of cones.

4.1.1. Eruption volumes and modes of emplacement

The clustered locations of cones at Butajira indicates differing behavior of dikes in the near surface compared to the isolated cones at East Ziway. Clusters can be formed either by dikes repeatedly using similar pathways, or by multiple cones being emplaced by the same dike. The lack of clearly overlapping deposits in cone geomorphology (deposits from each eruption location are inseparable; Fig. 3b) suggests that the cones were emplaced contemporaneously and the clusters were therefore formed by few/single events. This is supported by the consistent linear shape of each cluster. This suggests that the Butajira field has hosted larger eruptions, with cone cluster volumes ranging from at least 10^7 – 10^8 m³ (Fig. 5a), and associated lava flows building a broader topographic high as large as 4.6×10^8 m³ (Fig. S5).

Corazzato and Tibaldi (2006) proposed a morphological classification of cones on the basis of the coeval eruption points along the same magma-feeding fracture. Simple cones are formed from a single eruption point. A multiple superimposed cone (e.g., a cluster from the Butajira field) forms from numerous eruption points along the same fracture. A multiple rifted cone is a large, elongated ridge formed when craters at each eruption point coalesce entirely – an example is found in the east of the East Ziway area (Fig. 3d). Simple cones are fed by a fracture constrained by high stresses and/or low magma pressure (Corazzato and Tibaldi, 2006). With lower confining stresses and/or higher magma pressures, the fracture feeds a great number of eruption points with shorter separations, creating multiple superimposed cones or multiple rifted cones (Fig. 8; Corazzato and Tibaldi, 2006). This field evidence suggests that the Butajira field has been fed by fractures with generally lower confining stresses and/or higher magma pressures than the East Ziway field, except for the fracture that fed the multiple rifted cone in East Ziway. The confining stress can be considered as a superposition of the lithostatic pressure, the normal component of topographic stress and the far-field extensional stress (e.g., Maccaferri et al., 2015). It is possible that variations in confining stresses between off-rift volcanism at Butajira and the within-rift volcanism at East Ziway are related to their location with respect to the rift axis, and this in turn plays a role in modifying eruptive style. Further work is required to test this hypothesis.

Cones in both fields are preferentially located to the west of the east-dipping normal faults. Modelling studies suggest that topographic unloading during rift formation can lead to the formation of off-rift volcanism, due to dike deflection away from low topography (Maccaferri et al., 2014). Similarly, differential topographic loads of <100 m induced by individual normal faults can cause dike deflection and can be responsible for the emplacement of cones on the footwall (Maccaferri et al., 2015). Dike deflection may therefore explain the location of cones in the Butajira field, offset from the main depression of the Main Ethiopian Rift and ~2 km west of east-dipping normal faults (Fig. 8).

In East Ziway, the main rift depression is to the west and local normal faults have relatively small offsets. In contrast to the low number of faults at Butajira, the pervasive faulting and seismic activity in the WFB provide several competing pathways for magma ascent. It is possible that dikes are captured by these faults (e.g., Le Corvec et al., 2013b; Gaffney et al., 2007), and are deflected by the differential topographic load of the fault scarps only at shallow depths, creating small offsets to the west (Fig. 8). Further research is required to investigate the relative influences of faults on dikes and dikes on faults in these areas.

4.1.2. Lakes, groundwater and local hydrology

The central Main Ethiopian Rift hosts numerous lakes – in the present day these are mostly on the eastern side of the rift although a variable number of small, transient lakes are found within the horst and graben structures of the SDFZ. The lakes have developed through four stages from the Late Pleistocene onwards (100 ka; Gasse and Street,

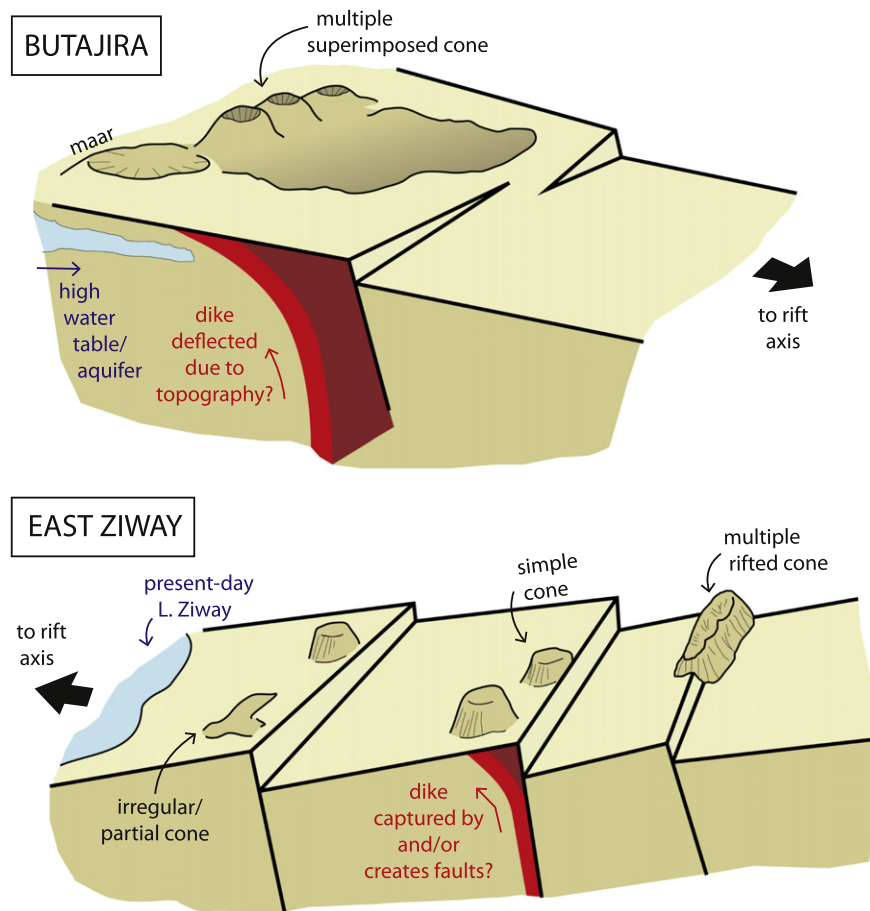


Fig. 8. Summary of the tectonic and hydrological contexts of the Butajira and East Ziway volcanic fields and their influence on cone/maar formation.

1978; Le Turdu et al., 1999; Benvenuti et al., 2002): (i) a megalake phase (Late Pleistocene, 100–22 ka), in which one lake covered much of the rift floor; (ii) a reduced-lake phase (latest Pleistocene, 22–10 ka) coinciding with the Last Glacial Maximum; (iii) a macrolake phase (early-mid Holocene, 10–5 ka), with lake connectivity limited by tectonic changes in topography; and (iv) the separated-lake phase (late Holocene-present, <5 ka). Large fluctuations in lake levels are common in all four phases (Benvenuti et al., 2002), fluctuating by as much as 120 m in the Holocene (Chalie and Gasse, 2002; Benvenuti et al., 2002, 2013).

Lacustrine sedimentation in East Ziway was significant during the megalake phase (Late Pleistocene), and restricted to the west of the cone field during the macrolake phase (early-mid Holocene). Sedimentation may have obscured evidence for small maars and other structures. However, the lack of any observable structures attributable to phreatomagmatic activity in East Ziway may indicate an absence of surface water in this area at time of eruption. This suggests that the East Ziway cones may have been emplaced during a dry phase, at a time of low lake level, perhaps prior to 100 ka (when estimates of lake extents are largely uncertain; Le Turdu et al., 1999), or during a later lake-level low stand.

In contrast, the presence of maars in the Butajira field indicates phreatomagmatic activity. One cone, BU34, possibly hosts a series of rootless cones (Fig. 3a), the evidence of which is outlined in Section 3.1, suggesting the presence of surface water. Phreatomagmatic activity may influence ratios of crater depth to cone height (D_{cr}/H_{co}) and the abundance of breached cones (Risso et al., 2008). Generally, phreatomagmatism results in lower and broader structures (e.g., Risso et al., 2008). Surface water and/or groundwater increases the explosivity of the eruption – the depth at which fragmentation occurs

may change depending on the depth of the groundwater/nearby aquifer, which may increase or decrease the depth of the crater and the likelihood of breaching the cone (e.g., Aranda-Gomez and Luhr, 1996; Risso et al., 2008).

The abundance of water in the Butajira area is evident in the present-day. The higher elevation on the rift flanks provides a wetter climate than the rift floor, and the nearby plateau and Guraghe mountains act as a major source of groundwater for the whole rift (Kebede et al., 2008; Bretzler et al., 2011). Accordingly, there are numerous small bodies of water, including the crater lake of Hare Sheitan within a maar structure (BU31e).

The morphology of the Butajira cone field indicates that the cones and maars were emplaced in a similarly wet environment to the present day, or wetter (Fig. 8). The hydrological context of rift-related cone fields is therefore key to morphological characteristics, eruptive process and associated hazards.

4.1.3. Relative ages of cones

There are few age constraints on the scoria cones of the Main Ethiopian Rift, and any indication of relative age is of great use in hazard assessment, as well as identifying the environment into which these cones were emplaced (e.g., Le Corvec et al., 2013c). Age is a significant control on cone morphometry, with progressive degradation leading to lower H_{max}/W_{co} values than the average for fresh cones of 0.18 (e.g., Inbar et al., 2011; Fig. 6). However, several recent studies suggest that other factors may dominate this ratio, including eruption dynamics, baseline topography and the exact method of calculating H_{max}/W_{co} (ratio of maximum height to average width; e.g., Favalli et al., 2009; Kervyn et al., 2012). The grainsize of the scoria comprising the cone is

a key parameter, which is also linked to explosivity and water content (e.g., Riedel et al., 2003).

The Butajira cones have higher H_{max}/W_{co} than those in East Ziway. Lake-sediment accumulation around the East Ziway cones may also have influenced their apparent heights and widths, perhaps contributing to low H_{max}/W_{co} ratios (Favalli et al., 2009) and an underestimation of cone volumes. The Butajira cones also have higher D_{cr}/H_{co} (ratio of crater depth to average height) than those in East Ziway. This may be influenced by phreatomagmatism (as discussed in Section 4.1.2). The Butajira cones also have sharper rims, with greater curvature on radial profiles, than those in East Ziway (Fig. 4b).

Higher H_{max}/W_{co} , lower D_{cr}/H_{co} and sharper rims in the Butajira cones are all consistent with a younger apparent age than for cones in East Ziway. The combination of factors provides a greater degree of confidence than any single factor. Potential differences in erosion process at each field prevents a quantitative assessment of the difference in age between cone fields, and the number of cones for which we can derive the parameters outlined above is low. Nonetheless, the cones at each field are separable using these parameters which suggests minimal overlap in ages between these fields. This hypothesis requires corroboration from absolute dating techniques.

Our data suggest that activity in the East Ziway area pre-dates that in the Butajira field. Since activity in the Butajira field is more recent, the possibility of ongoing activity cannot be ruled out. A recent magnetotelluric survey found a conductive body along the SDFZ to the east of Butajira (Hübert et al., 2018) and a diffuse CO₂ survey found elevated levels of magmatic degassing (Hunt et al., 2017). The current state of any magmatic reservoir in the area and the potential for future events is largely unknown.

In contrast, no magmatic degassing has been observed to the east of Aluto volcano, south of the East Ziway area in this study (Hunt et al., 2017). Successive magnetotelluric surveys have found no evidence for a conductor to the north east of Aluto towards East Ziway (Samrock et al., 2015; Hübert et al., 2018). This supports our hypothesis that activity at East Ziway precedes that of Butajira, and may have ceased.

4.2. Comparison of cone fields across the MER and other extensional environments

The comparison of morphometric parameters using the ASTER GDEM showed little systematic variation with cone field (Fig. S7, Fig. 7). The ASTER GDEM has insufficient resolution to categorize cones, and the analysis may include many irregular structures. The low resolution also leads to errors for each parameter, systematically underestimating H_{max}^{AS} and volume. These errors are volume-/size-dependent, with larger cones more accurately estimated (Fornaciai et al., 2012). Despite these shortcomings, a number of observations can be made. The variability of H_{max}^{AS} , W_{co}^{AS} , and volume for the Wonji field is greater than other fields. In contrast, the small volume fields north of Kone, south of Kone, and at Bishoftu exhibit a restricted range of H_{max}^{AS} and W_{co}^{AS} . The proximity of silicic volcanic centers (Gedemsa, Bora, Tullu Moje) and numerous lakes to the Wonji field may contribute to a greater variability in cone morphology due to partial burial. A relative lack of surface water/groundwater and lake sediment deposition in the north around Kone may contribute to accordingly less variability. This remains a hypothesis to test. Despite the difficulties of using low resolution DEMs, their wide coverage and free availability enables their use in comparing a large number of fields. As new global, free products at higher resolution become available (e.g., TanDEM-X; e.g., Albino et al., 2015; Bagnardi et al., 2016), morphometric comparisons of cones will provide useful insights into each cone field's characteristics.

Our analysis of rift-related volcanic fields using digital elevation models contributes to a growing literature on extension-related volcanic fields. Fornaciai et al. (2012) found that cones in extension-related fields have lower height to width (H/W) ratios and higher crater

width to cone width (W_{cr}/W_{co}) ratios than those in subduction-related fields. They speculated that higher water content in magma produced in subduction environments leads to greater explosivity and smaller grain size, which enables steeper sides to the cones (Riedel et al., 2003).

Our results show that cones in East Ziway have low H/W ratios, similar to many cone fields that show significant degradation (Fornaciai et al., 2012); this is probably the result of degradation rather than phreatomagmatism. Cones in Butajira have a range of H/W ratios, including values above those expected for freshly emplaced cones and at the highest end of values observed in either extension- or subduction-related fields (Fornaciai et al., 2012).

The cones in our analysis are smaller in volume ($\sim 4 \times 10^6 \text{ m}^3$) than those in a large number of fields from a variety of geodynamic environments ($\sim 9\text{--}96 \times 10^6 \text{ m}^3$; Fornaciai et al., 2012). Whilst erosion may have reduced the size of some cones, particularly in the East Ziway field, the low volumes calculated here may suggest that small pockets of melt are able to reach the surface with relative ease in the Main Ethiopian Rift compared to other environments. The complex interplay of stress, structures and hydrology in extensional environments strongly influence both the distribution and morphology of cones, and similar morphological studies in other rift settings would extend our understanding of these relationships.

5. Conclusions

The morphology of distributed volcanic fields in rift environments is influenced by a range of characteristic factors, including multiple generations of faults, repeated dike intrusions, an active hydrological cycle and rift development through time. In this study, we have presented new digital elevation models and compared the morphology of two distributed volcanic fields in the Main Ethiopian Rift, each hosting ca. 50 cones/maars.

Whilst average cone volumes are similar between the fields (mean $\sim 4 \times 10^6 \text{ m}^3$), smaller than in many fields worldwide, most other parameters differ significantly. The Butajira field hosts a mixture of maars and cones deposited in linear clusters of superimposed cones, whereas the East Ziway field comprises isolated cones and no maars (Fig. 8). Clusters at Butajira form part of a broader topographic high (volume $\sim 4.6 \times 10^8 \text{ m}^3$), possibly the result of lava flows and other volcanic deposits associated with the distributed cone field. The Butajira field is likely to have been fed by a few large fissure eruptions (cluster volumes $\sim 10^7\text{--}10^8 \text{ m}^3$), whereas the East Ziway field is the result of a larger number of small eruptions.

Maars and high D_{cr}/H_{co} ratios at Butajira suggest phreatomagmatic activity and the presence of surface water and/or groundwater, implying emplacement at a time when the local climate was at least as wet as the present day. At East Ziway, on the other hand, there is no evidence for phreatomagmatic activity despite the field's proximity to Lake Ziway. The cones were likely emplaced during a dry phase, although later lacustrine deposition may have buried maars and affected estimations of volume and cone height.

High H_{max}/W_{co} , D_{cr}/H_{co} and high negative curvature of cone rims all indicate a younger age of cones at Butajira compared to East Ziway. Despite an active volcanic center nearby in Aluto, the East Ziway field shows no sign of recent activity. Despite the main magmatic and tectonic activity of the rift migrating to the rift axis, ongoing activity at the Butajira field on the rift shoulder cannot be ruled out.

Analysis of other distributed volcanic fields across the MER using the ASTER GDEM is hindered by low-resolution, preventing classification of regular and irregular morphologies. The results from high-resolution DEMs in this study demonstrates the use of careful analysis of morphology to infer process and relative age of cones within the Main Ethiopian Rift. As higher resolution digital elevation models with large-scale, freely accessible coverage become available (e.g., TanDEM-X; e.g., Albino et al., 2015; Bagnardi et al., 2016), comparison of cone

morphology across rifts will grow our understanding of the interplay between cone morphology and rift environment.

Declaration of competing interest

The authors declare that they have no known competing financial interests or personal relationships that could have appeared to influence the work reported in this paper.

Acknowledgments

This work was supported by a studentship from NERC as part of the Environmental Research DTP (University of Oxford). This work is a contribution to the Natural Environment Research Council funded RiftVolc project (NE/L013932/1, Rift volcanism: past, present, and future). T.A.M., and D.M.P. are supported by and contribute to the NERC Centre for the Observation and Modelling of Earthquakes, Volcanoes, and Tectonics (COMET). We thank Giacomo Corti and one anonymous reviewer for their helpful comments.

Appendix A. Supplementary data

Supplementary data to this article can be found online at <https://doi.org/10.1016/j.jvolgeores.2019.106732>.

References

- Abebe, B., Acocella, V., Korme, T., Ayalew, D., 2007. Quaternary faulting and volcanism in the Main Ethiopian Rift. *J. Afr. Earth Sci.* 48 (2–3), 115–124. <https://doi.org/10.1016/j.jafrearsci.2006.10.005>.
- Abebe, T., Manetti, P., Bonini, M., Corti, G., Innocenti, F., Mazzarini, F., Pècksay, Z., 2005. Geological map (scale 1:200,000) of the northern Main Ethiopian Rift and its implications for the volcano-tectonic evolution of the rift. *Geological Society of America Map and Chart Series MCH094* (20 pp., doi: 110.1130/205GMOINMERTXT).
- Acocella, V., Korme, T., Salvini, F., Funicello, R., 2002. Elliptic calderas in the Ethiopian Rift: control of pre-existing structures. *J. Volcanol. Geotherm. Res.* 119 (1–4), 189–203. [https://doi.org/10.1016/S0377-0273\(02\)00342-6](https://doi.org/10.1016/S0377-0273(02)00342-6).
- Albert, H., Costa, F., Martí, J., 2016. Years to weeks of seismic unrest and magmatic intrusions precede monogenetic eruptions. *Geology* 44 (3), 211–214. <https://doi.org/10.1130/G37239.1>.
- Albino, F., Smets, B.N., d'Orey, N., Kervyn, F., 2015. High-resolution TanDEM-X DEM: an accurate method to estimate lava flow volumes at Nyamulagira Volcano (D. R. Congo). *Journal of Geophysical Research (Solid Earth)* 120, 4189–4207. <https://doi.org/10.1002/2015JB011988>.
- Armitage, J.J., Collier, J.S., Minshull, T.A., 2010. The importance of rift history for volcanic margin formation. *Nature* 465, 913–917. <https://doi.org/10.1038/nature09063>.
- Aranda-Gomez, J., Lühr, J.F., 1996. Origin of the Joya Honda maar, San Luis Potosi, México. *J. Volcanol. Geotherm. Res.* 74, 1–18.
- Bagnardi, M., González, P.J., Hooper, A., 2016. High-resolution digital elevation model from tri-stereo Pleiades-1 satellite imagery for lava flow volume estimates at Fogo Volcano. *Geophys. Res. Lett.* 43 (12), 6267–6275. <https://doi.org/10.1002/2016GL069457>.
- Bemis, K.G., Ferencz, M., 2017. Morphometric analysis of scoria cones: the potential for inferring process from shape. *Geol. Soc. Lond., Spec. Publ.* 446 (1), 61–100. <https://doi.org/10.1144/SP446.9>.
- Benvenuti, M., Carnicelli, S., Belluomini, G., Dainelli, N., Di Grazia, S., Ferrari, G.A., Iasio, C., Sagri, M., Ventura, D., Atnafu, B., Kebede, S., 2002. The Ziway-Shala lake basin (main Ethiopian rift, Ethiopia): a revision of basin evolution with special reference to the Late Quaternary. *J. Afr. Earth Sci.* 35 (2), 247–269. [https://doi.org/10.1016/S0899-5362\(02\)00036-2](https://doi.org/10.1016/S0899-5362(02)00036-2).
- Benvenuti, M., Bonini, M., Tassi, F., Corti, G., Sani, F., Agostini, A., Manetti, P., Vaselli, O., 2013. Holocene lacustrine fluctuations and deep CO₂ degassing in the northeastern Lake Langano Basin (Main Ethiopian Rift). *J. Afr. Earth Sci.* 77, 1–10. <https://doi.org/10.1016/j.jafrearsci.2012.09.001>.
- Bretzler, A., Osenbrück, K., Gloaguen, R., Ruprecht, J.S., Kebede, S., Stadler, S., 2011. Groundwater origin and flow dynamics in active rift systems - a multi-isotope approach in the Main Ethiopian Rift. *J. Hydrol.* 402 (3–4), 274–289. <https://doi.org/10.1016/j.jhydrol.2011.03.022>.
- Casey, M., Ebinger, C., Keir, D., Gloaguen, R., Mohamed, F., 2006. Strain accommodation in transitional rifts: extension by magma intrusion and faulting in Ethiopian rift magmatic segments. *Geol. Soc. Lond., Spec. Publ.* 259 (1), 143–163. <https://doi.org/10.1144/GSL.SP.2006.259.01.13>.
- Chalie, F., Gasse, F., 2002. Late Glacial-Holocene diatom record of water chemistry and lake level change from the tropical East African Rift Lake Abiyata (Ethiopia). *Palaeogeogr. Palaeoclimatol. Palaeoecol.* 187 (3–4), 259–283. [https://doi.org/10.1016/S0031-0182\(02\)00480-7](https://doi.org/10.1016/S0031-0182(02)00480-7).
- Chernet, T., Hart, W.K., Aronson, J.L., Walter, R.C., 1998. New age constraints on the timing of volcanism and tectonism in the northern Main Ethiopian Rift - southern Afar tran-
- sition zone (Ethiopia). *J. Volcanol. Geotherm. Res.* 80 (3–4), 267–280. [https://doi.org/10.1016/S0377-0273\(97\)00035-8](https://doi.org/10.1016/S0377-0273(97)00035-8).
- Condit, C.D., Connor, C.B., 1996. Recurrence rates of volcanism in basaltic volcanic fields: an example from the Springerville volcanic field, Arizona. *Bull. Geol. Soc. Am.* 108 (10), 1225–1241. [https://doi.org/10.1130/0016-7606\(1996\)108<1225:RROVIB>2.3.CO;2](https://doi.org/10.1130/0016-7606(1996)108<1225:RROVIB>2.3.CO;2).
- Connor, C.B., Conway, F.M., 2000. Basaltic volcanic fields. In: Sigurdsson, H. (Ed.), *Encyclopedia of Volcanoes*. Academic, New York, pp. 331–343.
- Connor, C.B., Condit, C.D., Crumpler, L.S., Aubele, J.C., 1992. Evidence of structural controls on Vent Distribution: Springerville Volcanic Field Arizona. *J. Geophys. Res.* 97 (B9), 12,349–12,359. <https://doi.org/10.1029/92JB00929>.
- Corazzato, C., Tibaldi, A., 2006. Fracture control on type, morphology and distribution of parasitic volcanic cones: an example from Mt. Etna, Italy. *J. Volcanol. Geotherm. Res.* 158, 177–194. <https://doi.org/10.1016/j.jvolgeores.2006.04.018>.
- Corti, G., 2008. Control of rift obliquity on the evolution and segmentation of the main Ethiopian rift. *Nat. Geosci.* 1 (4), 258–262. <https://doi.org/10.1038/ngeo160>.
- Corti, G., 2009. Continental rift evolution: from rift initiation to incipient break-up in the Main Ethiopian Rift, East Africa. *Earth Sci. Rev.* 96, 1–2, 1–53. <https://doi.org/10.1016/j.jearesciv.2009.06.005>.
- Corti, G., Bonini, M., Conticelli, S., Innocenti, F., Manetti, P., Sokoutis, D., 2003. Analogue modelling of continental extension: a review focused on the relations between the patterns of deformation and the presence of magma. *Earth Sci. Rev.* 63 (3–4), 169–247. [https://doi.org/10.1016/S0012-8252\(03\)00035-7](https://doi.org/10.1016/S0012-8252(03)00035-7).
- Corti, G., Sani, F., Philippon, M., Sokoutis, D., Willingshofer, E., Molin, P., 2013. Quaternary volcano-tectonic activity in the Soddio region, western margin of the Southern Main Ethiopian Rift. *Tectonics* 32 (4), 861–879. <https://doi.org/10.1002/tect.20052>.
- Corti, G., Molin, P., Sembroni, A., Bastow, I.D., Keir, D., 2018a. Control of pre-rift lithospheric structure on the architecture and evolution of continental rifts: insights from the Main Ethiopian Rift, East Africa. *Tectonics* 37, 477–496. <https://doi.org/10.1002/2017TC004799>.
- Corti, G., Sani, F., Agostini, S., Philippon, M., Sokoutis, D., Willingshofer, E., 2018b. Off-axis volcano-tectonic activity during continental rifting: Insights from the transversal Goba-Bonga lineament, Main Ethiopian Rift (East Africa). *Tectonophysics* 728–729, 75–91. <https://doi.org/10.1016/j.tecto.2018.02.011>.
- Daniels, K.A., Bastow, I.D., Keir, D., Sparks, R.S.J., Menand, T., 2014. Thermal models of dyke intrusion during development of continent-ocean transition. *Earth Planet. Sci. Lett.* 385, 145–153. <https://doi.org/10.1016/j.epsl.2013.09.018>.
- Ebinger, C.J., Casey, M., 2001. Continental breakup in magmatic provinces: an Ethiopian example. *Geology* 29 (6), 527–530. [https://doi.org/10.1130/0091-7613\(2001\)029-0527:CBIMPA>2.0.CO;2](https://doi.org/10.1130/0091-7613(2001)029-0527:CBIMPA>2.0.CO;2).
- Favalli, M., Karátson, D., Mazzarini, F., Pareschi, M.T., Boschi, E., 2009. Morphometry of scoria cones located on a volcano flank: a case study from Mt. Etna (Italy), based on high-resolution LiDAR data. *J. Volcanol. Geotherm. Res.* 186 (3–4), 320–330. <https://doi.org/10.1016/j.jvolgeores.2009.07.011>.
- Ferguson, D.J., MacLennan, J., Bastow, I.D., Pyle, D.M., Jones, S.M., Keir, D., Blundy, J.D., Plank, T., Yirgu, G., 2013. Melting during late-stage rifting in Afar is hot and deep. *Nature* 499, 70–74. <https://doi.org/10.1038/nature12292>.
- Fontijn, K., McNamara, K., Zafu Tadesse, A., Pyle, D.M., Dessalegn, F., Hutchison, W., Mather, T.A., Yirgu, G., 2018. Contrasting styles of post-caldera volcanism along the Main Ethiopian Rift: Implications for contemporary volcanic hazards. *J. Volcanol. Geotherm. Res.* 356, 90–113. <https://doi.org/10.1016/j.jvolgeores.2018.02.001>.
- Fornaciari, A., Favalli, M., Karátson, D., Tarquini, S., Boschi, E., 2012. Morphometry of scoria cones, and their relation to geodynamic setting: a DEM-based analysis. *J. Volcanol. Geotherm. Res.* 217–218, 56–72. <https://doi.org/10.1016/j.jvolgeores.2011.12.012>.
- Gaffney, E.S., Damjanac, B., Valentine, G.A., 2007. Localization of volcanic activity: 2. Effects of pre-existing structure. *Earth Planet. Sci. Lett.* 263 (3–4), 323–338. <https://doi.org/10.1016/j.epsl.2007.09.002>.
- Gasse, F., Street, F.A., 1978. Late Quaternary lake-level fluctuations and environments of the northern Rift Valley and Afar region (Ethiopia and Djibouti). *Palaeogeogr. Palaeoclimatol. Palaeoecol.* 24, 279–325. [https://doi.org/10.1016/0031-0182\(78\)90011-1](https://doi.org/10.1016/0031-0182(78)90011-1).
- Hayward, N.J., Ebinger, C.J., 1996. Variations in the along-axis segmentation of the Afar Rift system. *Tectonics* 15 (2), 244–257. <https://doi.org/10.1029/95TC02292>.
- Inbar, M., Gilichinsky, M., Melekestev, I., Melnikov, D., Zaretskaya, N., 2011. Morphometric and morphological development of Holocene cinder cones: A field and remote sensing study in the Tolbachik volcanic field, Kamchatka. *J. Volcanol. Geotherm. Res.* 201, 301–311. <https://doi.org/10.1016/j.jvolgeores.2010.07.013>.
- Hübert, J., Whaler, K., Fisseha, S., 2018. The electrical structure of the central main Ethiopian Rift as imaged by magnetotellurics: implications for magma storage and pathways. *Journal of Geophysical Research: Solid Earth* 123 (7), 6019–6032. <https://doi.org/10.1029/2017JB015160>.
- Hughes, S.S., Wetmore, P.H., Casper, J.L., 2002. Evolution of Quaternary tholeiitic basalt eruptive centers on the eastern Snake River Plain, Idaho. *Idaho Geological Survey Bulletin* 30, 1–23.
- Hunt, J.A., Zafu Tadesse, A., Mather, T.A., Pyle, D.M., Barry, P.H., 2017. Spatially variable CO₂ degassing in the Main Ethiopian Rift: implications for magma storage, volatile transport, and rift-related emissions. *Geochem. Geophys. Geosyst.* 18, 1–24. <https://doi.org/10.1002/2017GC006975>.
- Hutchison, W., Pyle, D.M., Mather, T.A., Yirgu, G., Biggs, J., Cohen, B.E., Barford, D.N., Lewi, E., 2016. The eruptive history and magmatic evolution of Aluto volcano: new insights into silicic peralkaline volcanism in the Ethiopian Rift. *J. Volcanol. Geotherm. Res.* 328, 9–33. <https://doi.org/10.1016/j.jvolgeores.2016.09.010>.
- Kebede, S., Travi, Y., Asrat, A., Alemayehu, T., Ayenew, T., Tessema, Z., 2008. Groundwater origin and flow along selected transects in Ethiopian Rift volcanic aquifers. *Hydrogeol. J.* 16, 55–73. <https://doi.org/10.1007/s10040-007-0210-0>.

- Keir, D., Ebinger, C.J., Stuart, G.W., Daly, E., Ayele, A., 2006. Strain accommodation by magmatism and faulting as rifting proceeds to breakup: seismicity of the northern Ethiopian rift. *Journal of Geophysical Research: Solid Earth* 111 (5), 1–17. <https://doi.org/10.1029/2005JB003748>.
- Keir, D., Hamling, I.J., Ayele, A., Calais, E., Ebinger, C., Wright, T.J., Jacques, E., Mohamed, K., Hammond, J.O.S., Belachew, M., Baker, E., Rowland, J.V., Lewi, E., Bennati, L., 2009. Evidence for focused magmatic accretion at segment centers from lateral dike injections captured beneath the Red Sea rift in Afar. *Geology* 37 (1), 59–62. <https://doi.org/10.1130/G25147A.1>.
- Kendall, J.M., Stuart, G.W., Ebinger, C.J., Bastow, I.D., Keir, D., 2005. Magma-assisted rifting in Ethiopia. *Nature* 433 (7022), 146–148. <https://doi.org/10.1038/nature03161>.
- Kereszturi, G., Németh, K., Csillag, G., Balogh, K., Kovács, J., 2011. The role of external environmental factors in changing eruption styles of monogenetic volcanoes in a Mio/Pleistocene continental volcanic field in western Hungary. *J. Volcanol. Geotherm. Res.* 201 (1–4), 227–240. <https://doi.org/10.1016/j.jvolgeores.2010.08.018>.
- Kervyn, M., Ernst, G.G.J., Carracedo, J.C., Jacobs, P., 2012. Geomorphometric variability of “monogenetic” volcanic cones: evidence from Mauna Kea, Lanzarote and experimental cones. *Geomorphology* 136 (1), 59–75. <https://doi.org/10.1016/j.geomorph.2011.04.009>.
- Korme, T., Chorowicz, J., Collet, B., Bonavia, F.F., 1997. Volcanic vents rooted on extension fractures and their geodynamic implications in the Ethiopian Rift. *J. Volcanol. Geotherm. Res.* 79 (3–4), 205–222. [https://doi.org/10.1016/S0377-0273\(97\)00034-6](https://doi.org/10.1016/S0377-0273(97)00034-6).
- Korme, T., Acocella, V., Abebe, B., 2004. The role of pre-existing structures in the origin, propagation and architecture of faults in the Main Ethiopian Rift. *Gondwana Res.* 7 (2), 467–479. [https://doi.org/10.1016/S1342-937X\(05\)70798-X](https://doi.org/10.1016/S1342-937X(05)70798-X).
- Le Corvec, N., Spörl, K.B., Rowland, J., Lindsay, J., 2013a. Spatial distribution and alignments of volcanic centers: clues to the formation of monogenetic volcanic fields. *Earth Sci. Rev.* 124, 96–114. <https://doi.org/10.1016/j.earscirev.2013.05.005>.
- Le Corvec, N., Menand, T., Lindsay, J., 2013b. Interaction of ascending magma with pre-existing crustal fractures in monogenetic basaltic volcanism: an experimental approach. *Journal of Geophysical Research: Solid Earth* 118 (3), 968–984. <https://doi.org/10.1002/jgrb.50142>.
- Le Corvec, N., Bebbington, M.S., Lindsay, J.M., McGee, L.E., 2013c. Age, distance, and geochemical evolution within a monogenetic volcanic field: analyzing patterns in the Auckland Volcanic Field eruption sequence. *Geochem. Geophys. Geosyst.* 14 (9), 3648–3665. <https://doi.org/10.1002/ggge.20223>.
- Le Turdu, C., Tiercelin, J.-J., Gibert, E., Travi, Y., Lezzar, K.-E., Richert, J.-P., Massault, M., Gasse, F., Bonnefille, R., Decobert, M., Gensous, B., Jeudy, V., Tamrat, E., Mohammed, M.U., Martens, K., Atnafu, B., Chernet, T., Williamson, D., Taieb, M., 1999. The Ziway-Shala lake basin system, Main Ethiopian Rift: influence of volcanism, tectonics, and climatic forcing on basin formation and sedimentation. *Palaeogeogr. Palaeoclimatol. Palaeoecol.* 150, 135–177. [https://doi.org/10.1016/S0031-0182\(98\)00220-X](https://doi.org/10.1016/S0031-0182(98)00220-X).
- Maccaferri, F., Rivalta, E., Keir, D., Acocella, V., 2014. Off-rift volcanism in rift zones determined by crustal unloading. *Nat. Geosci.* 7 (4), 297–300. <https://doi.org/10.1038/ngeo2110>.
- Maccaferri, F., Acocella, V., Rivalta, E., 2015. How the differential load induced by normal fault scarps controls the distribution of monogenic volcanism. *Geophys. Res. Lett.* 42 (18), 7507–7512. <https://doi.org/10.1002/2015GL065638>.
- Mazzarini, F., Isola, I., 2010. Monogenetic vent self-similar clustering in extending continental crust: examples from the East African Rift System. *Geosphere* 6 (5), 567–582. <https://doi.org/10.1130/GES00569.1>.
- Mazzarini, F., Abebe, T., Innocenti, F., Manetti, P., Pareschi, M.T., 1999. *Geology of the Debre Zeyt area (Ethiopia) (with a geologic map at scale 1:100,000)*. *Acta Vulcanologica* 11, 131–141.
- Mazzarini, F., Keir, D., Isola, I., 2013a. Spatial relationship between earthquakes and volcanic vents in the central-northern Main Ethiopian Rift. *J. Volcanol. Geotherm. Res.* 262, 123–133. <https://doi.org/10.1016/j.jvolgeores.2013.05.007>.
- Mazzarini, F., Rooney, T.O., Isola, I., 2013b. The intimate relationship between strain and magmatism: a numerical treatment of clustered monogenetic fields in the Main Ethiopian Rift. *Tectonics* 32 (1), 49–64. <https://doi.org/10.1029/2012TC003146>.
- Mazzarini, F., Le Corvec, N., Isola, I., Favalli, M., 2016. Volcanic field elongation, vent distribution, and tectonic evolution of a continental rift: the Main Ethiopian Rift example. *Geosphere* 12 (3), 706–720. <https://doi.org/10.1130/GES01193.1>.
- McNamara, K., Cashman, K.V., Rust, A.C., Fontijn, K., Chalié, F., Tomlinson, E.L., Yirgu, G., 2018. Using lake sediment cores to improve records of volcanism at Aluto volcano in the Main Ethiopian Rift. *Geochem. Geophys. Geosyst.* 19 (9), 3164–3188. <https://doi.org/10.1029/2018GC007686>.
- Michon, L., Merle, O., 2001. The evolution of the Massif Central rift: spatio-temporal distribution of the volcanism. *Bulletin de La Société Géologique de France* 172 (2), 201–211. <https://doi.org/10.2113/172.2.201>.
- Muirhead, J.D., Kattenhorn, S.A., Le Corvec, N., 2015. Varying styles of magmatic strain accommodation across the East African Rift. *Geochem. Geophys. Geosyst.* 16, 2775–2795. <https://doi.org/10.1002/2015GC005918>.
- Muirhead, J.D., Van Eaton, A.R., Re, G., White, J.D.L., Ort, M.H., 2016. Monogenetic volcanoes fed by interconnected dikes and sills in the Hopi Buttes volcanic field, Navajo Nation, USA. *Bulletin of Volcanology* 78 (2), 11. <https://doi.org/10.1007/s00445-016-1005-8>.
- Paulsen, T.S., Wilson, T.J., 2010. New criteria for systematic mapping and reliability assessment of monogenetic volcanic vent alignments and elongate volcanic vents for crustal stress analyses. *Tectonophysics* 482 (1–4), 16–28. <https://doi.org/10.1016/j.tecto.2009.08.025>.
- Porter, S.C., 1972. Distribution, morphology, and size frequency of cinder cones on Mauna Kea Volcano, Hawaii. *Geol. Soc. Am. Bull.* 83 (12), 3607–3612. [https://doi.org/10.1130/0016-7606\(1972\)83\[3607:DMASFO\]2.0.CO;2](https://doi.org/10.1130/0016-7606(1972)83[3607:DMASFO]2.0.CO;2).
- Riedel, C., Ernst, G.G.J., Riley, M., 2003. Controls on the growth and geometry of pyroclastic constructs. *J. Volcanol. Geotherm. Res.* 127, 121–152. [https://doi.org/10.1016/S0377-0273\(03\)00196-3](https://doi.org/10.1016/S0377-0273(03)00196-3).
- Risso, C., Németh, K., María, A., Nullo, F., Drosina, M., 2008. The role of phreatomagmatism in a Plio-Pleistocene high-density scoria cone field: Llancanelo Volcanic Field (Mendoza), Argentina. *J. Volcanol. Geotherm. Res.* 169, 61–86. <https://doi.org/10.1016/j.jvolgeores.2007.08.007>.
- Rooney, T., Furman, T., Bastow, I., Ayalew, D., Yirgu, G., 2007. Lithospheric modification during crustal extension in the Main Ethiopian Rift. *J. Geophys. Res.* 112 (B10201). <https://doi.org/10.1029/2006JB004916>.
- Rooney, T.O., Furman, T., Yirgu, G., Ayalew, D., 2005. Structure of the Ethiopian lithosphere: xenolith evidence in the Main Ethiopian Rift. *Geochim. Cosmochim. Acta* 69 (15), 3889–3910. <https://doi.org/10.1016/j.gca.2005.03.043>.
- Rooney, T.O., Bastow, I.D., Keir, D., 2011. Insights into extensional processes during magma assisted rifting: evidence from aligned scoria cones. *J. Volcanol. Geotherm. Res.* 201 (1–4), 83–96. <https://doi.org/10.1016/j.jvolgeores.2010.07.019>.
- Rooney, T.O., Bastow, I.D., Keir, D., Mazzarini, F., Movsesian, E., Grosfils, E.B., Zimbelman, J.R., Ramsey, M.S., Ayalew, D., Yirgu, G., 2014. The protracted development of focused magmatic intrusion during continental rifting. *Tectonics* 33, 875–897. <https://doi.org/10.1002/2013TC003514> (Received).
- Samrock, F., Kuvshinov, A., Bakker, J., Jackson, A., Fisseha, S., 2015. 3-D analysis and interpretation of magnetotelluric data from the Aluto-Langano geothermal field, Ethiopia. *Geophys. J. Int.* 202 (3), 1923–1948. <https://doi.org/10.1093/gji/ggv270>.
- Settle, M., 1979. The structure and emplacement of cinder cone fields. *Am. J. Sci.* 279, 1089–1107. <https://doi.org/10.2475/ajs.279.10.1089>.
- Smith, I.E.M., Németh, K., 2017. Source to surface model of monogenetic volcanism: a critical review. *Geol. Soc. Lond., Spec. Publ.* 446 (1), 1–28. <https://doi.org/10.1144/SP446.14>.
- Tibaldi, A., 1995. Morphology of pyroclastic cones and tectonics. *J. Geophys. Res.* 100 (B12), 24521–24535. <https://doi.org/10.1029/95JB02250>.
- WoldeGabriel, G., Aronson, J.L., Walter, R.C., 1990. Geochronology and rift basin development in the central sector of the Main Ethiopian Rift. *Geol. Soc. Am. Bull.* 102 (4), 439–485. [https://doi.org/10.1130/0016-7606\(1990\)102<0439>](https://doi.org/10.1130/0016-7606(1990)102<0439>).
- Wolfenden, E., Ebinger, C., Yirgu, G., Deino, A., Ayalew, D., 2004. Evolution of the northern Main Ethiopian rift: birth of a triple junction. *Earth Planet. Sci. Lett.* 224 (1–2), 213–228. <https://doi.org/10.1016/j.epsl.2004.04.022>.
- Wood, C.A., 1980a. Morphometric evolution of cinder cones. *J. Volcanol. Geotherm. Res.* 7, 387–413. [https://doi.org/10.1016/0377-0273\(80\)90040-2](https://doi.org/10.1016/0377-0273(80)90040-2).
- Wood, C.A., 1980b. Morphometric analysis of cinder cone degradation. *J. Volcanol. Geotherm. Res.* 8, 137–160. [https://doi.org/10.1016/0377-0273\(80\)90101-8](https://doi.org/10.1016/0377-0273(80)90101-8).
- Wright, T.J., Ebinger, C., Biggs, J., Ayele, A., Yirgu, G., Keir, D., Stork, A., 2006. Magma-maintained rift segmentation at continental rupture in the 2005 Afar dyking episode. *Nature* 442 (7100), 291–294. <https://doi.org/10.1038/nature04978>.
- Zhou, Y., Parsons, B., Elliott, J.R., Barisin, I., Walker, R.T., 2015. Assessing the ability of Pleiades stereo imagery to determine height changes in earthquakes: a case study for the El Mayor-Cucapah epicentral area. *Journal of Geophysical Research: Solid Earth* 120 (12), 8793–8808. <https://doi.org/10.1002/2015JB012358>.